Interlayer states arising from anionic electrons in the honeycomb-lattice-based compounds *Ae*AlSi (*Ae* = Ca, Sr, Ba)

Yangfan Lu,[1,2] Tomofumi Tada,[1,2] Yoshitake Toda,[1,2] Shigenori Ueda,[3,4] Jiazhen Wu,[1,2] Jiang Li,[1,2] Koji Horiba,[5] Hiroshi Kumigashira,[5] Yaoqing Zhang,[1,2] and Hideo Hosono[1,2,*]

[1]*Materials Research Center for Element Strategy, Tokyo Institute of Technology, 4259 Nagatsuta, Midori-ku, Yokohama 226-8503, Japan*
[2]*ACCEL, Japan Science and Technology Agency (JST), 4-1-8 Honcho, Kawaguchi, Saitama 332-0012, Japan*
[3]*Synchrotron X-ray Station at SPring-8, National Institute for Material Science (NIMS), 1-1-1 Kouto, Sayo, Hyogo 679-5148, Japan*
[4]*Quantum Beam Unit, NIMS, 1-2-1 Sengen, Tsukuba 305-0047, Japan*
[5]*Photon Factory and Condensed Matter Research Center, Institute of Materials Structure Science, High Energy Accelerator Research Organization (KEK), 1-1 Oho, Tsukuba 305-0801, Japan*

(Received 2 September 2016; revised manuscript received 12 January 2017; published 13 March 2017)

We report that the interlayer states common to the compounds *Ae*AlSi (*Ae* = Ca, Sr, Ba) arise from F-center-like electrons arrayed in periodic cavities. The SrPtSb-type intermetallic phases exhibit electrons localized to columns of the trigonal bipyramidal Ae_3Al_2 cages running perpendicular to the honeycomb layers. *Ab initio* calculations in combination with hard/soft x-ray photoemission spectroscopic measurements reveal that these features correspond to the anionic electrons that hybridize with apical Al $3p_z$ orbitals from the honeycomb layers above and below. Extra bands with a significant dispersion along the k_z direction therefore contribute to the Fermi level in contrast to the apparent two-dimensional connectivity of the bonding in the compounds, and completely account for the presence of interlayer states. Our study demonstrates how the cage centers may serve as electronically important crystallographic sites, and extend the anionic electron concept into honeycomb lattice compounds.

DOI: 10.1103/PhysRevB.95.125117

I. INTRODUCTION

Honeycomb lattice compounds have drawn considerable attention in the field of condensed matter physics over the past decades. In addition to a variety of quantum transport properties [1,2], many materials with related structures exhibit superconducting transitions with relatively high critical temperatures, as was reported for MgB_2 [3], *Ae*AlSi (*Ae* = Ca, Sr, Ba) [4,5], and graphite-intercalated compounds (GICs) [6–8]. One of the most intriguing electronic features particular to these systems is the presence of interlayer states. It was first reported in bulk graphite that some of its bands exhibit anomalously large dispersion along the k_z direction, in stark contrast to the two-dimensional character of the σ and π bands [9,10]. While the interlayer state is located above the Fermi level in graphite, it hosts a finite number of electrons in electron-doped GICs [11,12] and *Ae*AlSi [13–16]. Remarkably, these states do not always passively hold electrons, but can play a critical role in Cooper pairing through π^*-interlayer interactions [17] and strong electron-phonon coupling [11,12,18,19].

Recognizing their uniqueness with regard to chemical bonding and their relevance for Cooper pairing mechanisms, various studies have been performed to determine the electronic origins of the interlayer states in GICs and *Ae*AlSi. At present, two proposed scenarios are prevailing. The first model attributes these bands with three-dimensional character to *sd*-like electrons on the intercalated metals, such as Ca [12,13,18,20,21] and rare-earth elements [22]. The alternative scenario, on the other hand, focuses on the contributions from p_z orbitals of the atoms forming the honeycomb network [14,15]. Both of them provide electronic explanations for the unexpectedly high interlayer coupling in the band structures. However, it is unlikely these extra electronic states are due to intercalated metals, as they are also present in metal-free graphite [9,10]. Furthermore, the interlayer distances are too large for chemical bond formation in these systems, leaving open the question of their electronic origin. The elucidation of these unconventional states would therefore provide new insights into the electronic structures of honeycomb lattice systems.

The *Ae*AlSi families of compounds are one of the simplest systems with such interlayer states crossing the Fermi energies. Here, we focus on both *Ae*AlSi and their hydrides, *Ae*AlSiH, and discuss how the interlayer states can be interpreted in terms of periodic F centers. All three of the *Ae*AlSi phases will be revealed to host electron density peaks in the vacant spaces (Ae_3Al_2 cage) originally occupied by H^- ions in *Ae*AlSiH. As the F-center states are of *s*-orbital character when the electron density is less than two per vacant site [23,24], anionic electrons in the Ba_3Al_2 cage should exhibit σ bonding interaction with apical Al $3p_z$ orbitals of the neighboring honeycomb layers. This gives rise to bands with free-electron-like character along the k_z direction, i.e., the interlayer states. These energy states are independent of the particular elements involved, but are sensitive to site occupancy, as they vanish when hydrogen atoms are incorporated into the vacant space. The *Ae*AlSi family therefore appears to offer a valuable lesson in how periodic cavities can be electronically important crystallographic sites even without nuclei.

II. EXPERIMENT AND CALCULATION METHOD

Polycrystalline *Ae*AlSi samples were synthesized using the arc-melting method under an argon atmosphere. The

*hosono@msl.titech.ac.jp

Ae, Al, and Si ingots were placed in a stoichiometric ratio on a water-cooled copper hearth and melted several times to ensure homogeneity. The weight losses after the melting processes were ∼3 wt.%. Powder x-ray diffraction (XRD) patterns were collected on a Bruker D8 Advance diffractometer with Cu Kα radiation at room temperature, and analyzed using RIETAN-FP [25] and VESTA [26].

Density functional theory (DFT) calculations were performed using the generalized gradient approximation with the Perdew-Burke-Ernzerhof (PBE96) functional and the projector augmented plane wave method, as implemented in the Vienna *ab initio* simulation package (VASP 5.2) [27,28]. The lattice parameters of *Ae*AlSiH and *Ae*AlSi were optimized using the force minimization methods to check consistency with experimental values before electronic structure calculations. The threshold value of forces acting on atoms for structural relaxation was set to 0.008 eV/Å, and the optimized lattice parameters agree well with refined data (Table I in Appendix A). The plane wave cutoff was set to 520 eV, and 12 × 12 × 11 of gamma-centered k mesh was used for self-consistent calculations.

To estimate the contributions from anionic electrons in the band structure and the projected density of states (PDOS), we employed the method proposed by Lee *et al.* [29]. The charge density was decomposed over the atom-centered spherical harmonics with a Wigner-Seitz radius $r_{\mathrm{WS}} = (3\,V_{\mathrm{cell}}/4\,\pi\,N)^{1/3}$ where V_{cell} and N are the unit cell volume and the number of atoms in a unit cell, respectively. Here we consider the vacant site X as an empty sphere which serves as an additional crystallographic site, and the N value was therefore set to $N = 4$ for *Ae*AlSi.

Hard x-ray photoemission spectroscopy (HAXPES) spectra were measured with the undulator beamline BL15XU of SPring-8 utilizing 6 keV x rays at room temperature [30,31]. The base pressure of the HAXPES chamber attached to a hemispherical electron analyzer (VG Scienta R4000) was lower than 1×10^{-7} Pa. Soft x-ray photoemission spectroscopy (SXPES) measurements were carried out using synchrotron radiation light at the beamline BL-2A MUSASHI of Photon Factory, KEK. For both measurements, the fresh sample surfaces were prepared by the fracturing *in situ*, and the binding energy is referred to the Fermi energy of a thin film of gold.

III. RESULTS AND DISCUSSION

The *Ae*AlSi compounds crystallize in the SrPtSb-type structure and can be viewed as metal-sandwiched variants of a honeycomb lattice [see Fig. 1(a)]. Our Rietveld refinements show that the interlayer distance between the Al atoms is as long as 4.4 Å in CaAlSi, and is further increased to 4.7 Å and 5.1 Å in SrAlSi and BaAlSi (see Fig. 6 in Appendix A). Even with the presence of the *Ae* atoms, this large distance between layers leaves open significant interstitial spaces, denoted as X in Fig. 1(a), which will be especially interesting to us in this study. Geometrically, the site X is located in a trigonal bipyramidal Ae_3Al_2 cage with the fractional coordinates of (2/3, 1/3, 0), and hosts a hydrogen atom in hydride forms of *Ae*AlSi as shown in the Fig. 1(b).

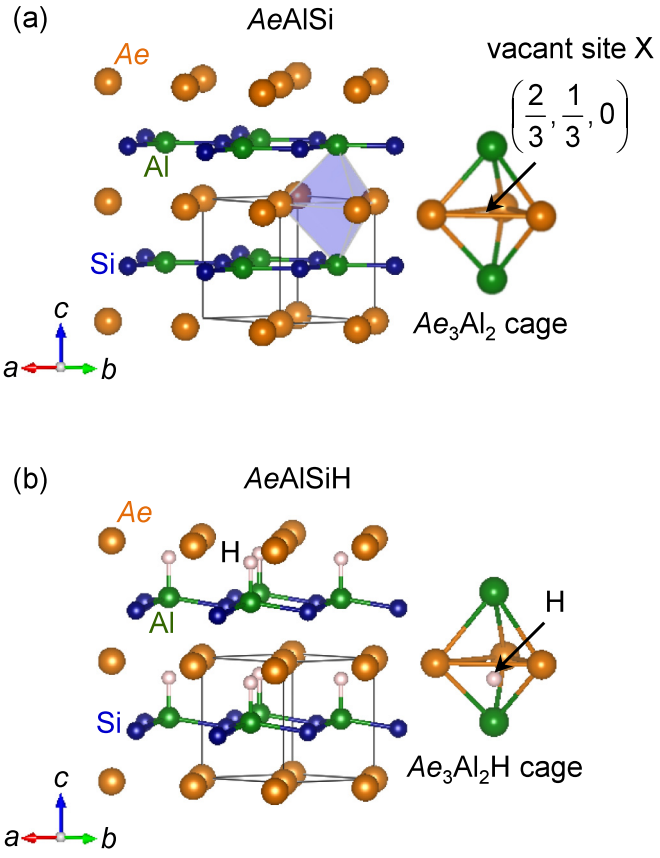

FIG. 1. (a) The crystal structure of *Ae*AlSi. *Ae*, Al, and Si atoms are depicted using orange, green, and dark blue spheres. The fractional coordinates of the *Ae*, Al, and Si sites are (0, 0, 0), (2/3, 1/3, 1/2), and (1/3, 1/3, 1/2), respectively. The Ae_3Al_2 cage is shown with a light blue polyhedron, and the vacant site in the Ae_3Al_2 cage, denoted as X, is indicated with a black arrow. The site X is located between interlayer Al atoms at the coordinates (2/3, 1/3, 0). (b) The crystal structure of *Ae*AlSiH. One hydrogen atom is incorporated into the Ae_3Al_2 cage as emphasized using the black arrow.

While the honeycomb lattice layer slightly distorts along the c axis after hydrogenation, the chemical bonding character appears to remain largely unchanged between the Al and Si atoms.

To understand the relationships between the bonding in *Ae*AlSi phases and their hydrides in more detail, we calculated the band structures of both BaAlSi and BaAlSiH with DFT. We begin with BaAlSiH since it can be viewed as a parent phase to BaAlSi. As is seen in Figs. 2(a) and 2(d), BaAlSiH is predicted to exhibit semiconducting character with an indirect band gap of ∼0.8 eV. The valence bands are composed of 3s and 3p orbitals of Al/Si, which overlap with each other to constitute three bonding σ bands and one π band. The H 1s orbital, exhibiting a small degree of mixing with the π band, mainly contributes to the band appearing at ∼5 eV below the Fermi level. These results roughly yield a formal valence state configuration of $[\mathrm{BaAlSi}]^{+}(\mathrm{H}^{-})$. The lowest conduction band of BaAlSiH, on the other hand, mainly originates from the antibonding π^* band of Al/Si 3p_z orbitals, which are further destabilized by antibonding contributions

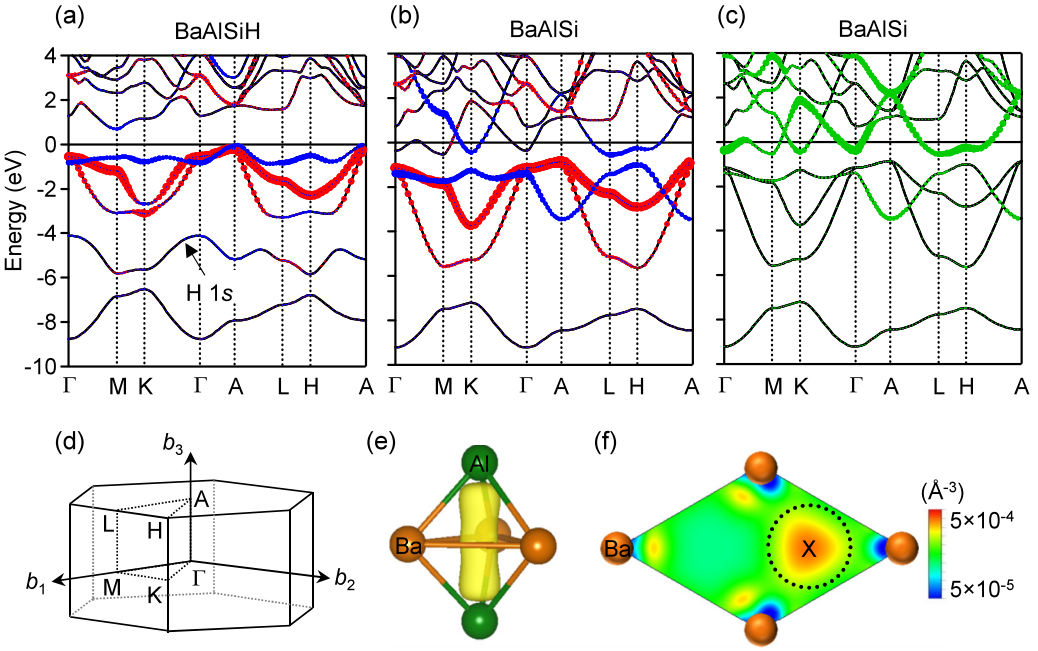

FIG. 2. (a) The band structure of BaAlSiH. The Al/Si $3p_{x,y}$ and $3p_z$ related bands are depicted using red and blue dots. (b) The band structure of hydrogen-free BaAlSi with emphasis on the Al/Si $3p_{x,y}$ (red dots) and $3p_z$ (blue dots) orbitals and (c) the vacant site X. The contribution from anionic electrons is represented using green dots. (d) The geometry of the first Brillouin zones of both BaAlSiH and BaAlSi. (e) The electron density of BaAlSi isolated in the Ba_3Al_2 cage shown with an isosurface of 4×10^{-4} electrons Å^{-3}. (f) The electron density map projected onto the (001) face of BaAlSi. In (e) and (f), the electron density distributions were calculated for states in the energy range of $-0.05 < E - E_F < 0.05$ eV.

from the H 1*s* orbitals below in the band structure. Because BaAlSiH accommodates ten valence electrons, the five valence bands (three from the Al-Si σ bonds, one for the hydride 1*s* orbital, and one from Al-Si π-bonding orbitals) are fully occupied, and the energy splitting between the valence and the π^* bands corresponds to the band gap of the system. It is noted that the lattice distortion does not significantly influence the fundamental electronic structures in this systems: the DFT calculation on the hypothetical BaAlSiH (with plane Al/Si layer) revealed that the lattice distortion solely narrows the energy width of σ and π bands due to reduced orbital overlap, whereas the number of electronic states remains unchanged (Fig. 7 in Appendix B). More importantly, no interlayer states can be observed below and above the Fermi level in both distorted (real) and nondistorted (hypothetical) BaAlSiH.

The calculated band structure of hydrogen-free BaAlSi, by contrast, is metallic with bands crossing the Fermi level [Figs. 2(b)–2(d)]. As extracting a hydrogen anion (H^-) as H^0 is equivalent to electron doping, the extra electrons would be transferred into the conduction band of BaAlSiH, at least within the framework of the rigid band model [14,32]. The actual situation for BaAlSi, however, is more interesting: a new band emerges that crosses the Fermi level, as is emphasized by green dots in Figs. 2(b) and 2(c). A comparison with Fig. 2(a) shows that the *k* dependence of this new band is different from any of those in semiconducting BaAlSiH. The vacant site X hosts an electron density peak which coincides with the formation of these unusually disperse bands, suggesting the possibility that these two unique features of the compound may be related [see Figs. 2(e) and 2(f)]. By integrating the electron density within empty spheres (with the Wigner-Seitz radius of $r_{WS} = 1.71$ Å for BaAlSi) at the site X, one can estimate their contributions in the band structure [Fig. 2(c)] as well as projected density of states (PDOS). The vacant electrons can be assigned to the new bands (green dots), and the calculated PDOS shows that one Ba_3Al_2 cage hosts ~0.9 electrons in the energy range of -12 eV $< E - E_F < 0$ eV, implying that electrons, doped by eliminating H^- ions, are not transferred into any particular atomic orbitals, but retained in the vacant site. These results are in contrast to the previously discussed electronic picture in which *Ae sd* [13] or Al/Si $3p_z$ orbitals [14,15] dominate the Fermi level in *Ae*AlSi. We argue that electrons in the Ba_3Al_2 cages occupy the fourth crystallographic site in the structure alongside the Ba, Al, and Si sites, leading to an extra band in BaAlSi that may be equated with the interlayer states of this compound.

We note that such electronic energy states contained with vacant sites are reminiscent of the F centers of ionic structures. As is frequently observed in oxide and halide insulators, electrons occupy anionic vacancy sites in an *s*-like orbital, giving rise to defect levels within the band gap [23,24]. In BaAlSi, on the other hand, the X sites create an array with perfect periodicity once all of the H^- ions are eliminated. Additional energy states arising from anionic electrons are therefore well defined in the momentum space, but are not associated with any particular atomic orbitals. Remarkably, due to the narrow gap semiconducting feature in the parent phase, the F-center state overlaps with the conduction band

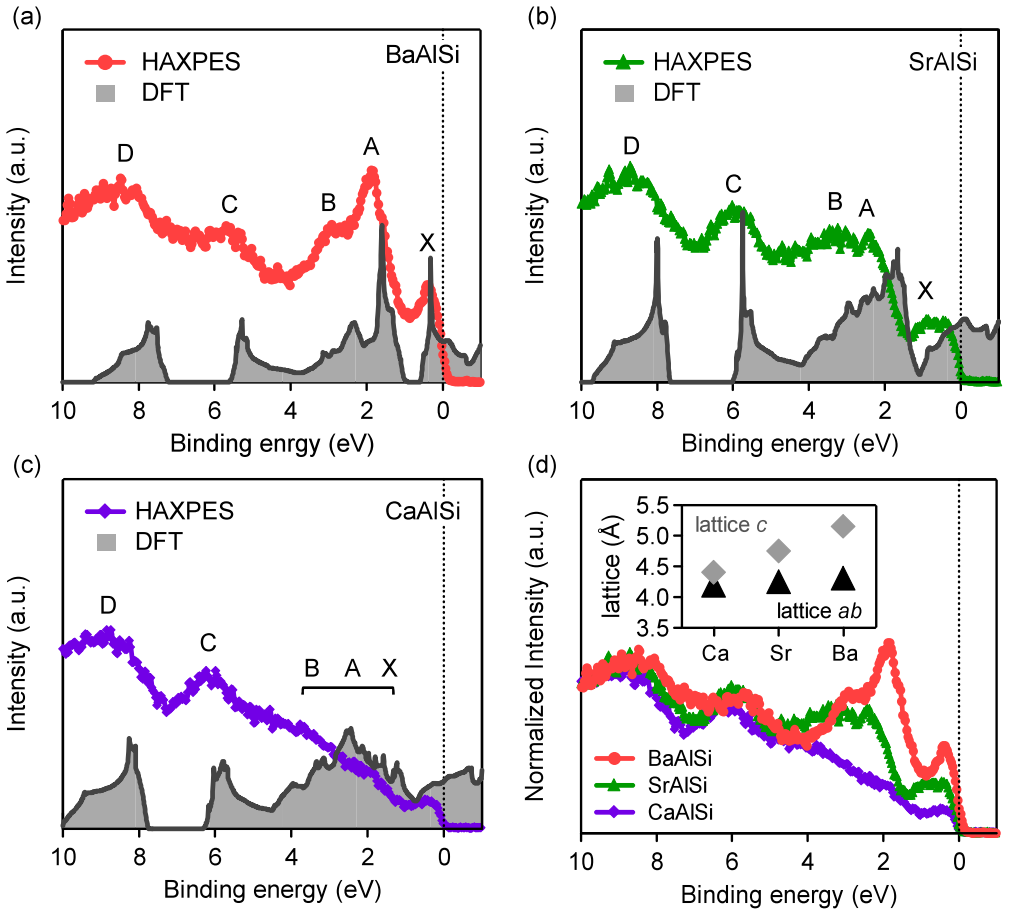

FIG. 3. The valence band HAXPES spectra taken at room temperature using polycrystalline (a) BaAlSi, (b) SrAlSi, and (c) CaAlSi, shown alongside the calculated total DOS. The energy of the incident x rays used was approximately 6 keV, and the escape depth of photoelectrons is on the order of ∼10 nm. The peaks derived from the anionic, Al/Si 3*s* and 3*p* electrons are denoted as X, A, B, C, and D. (d) The valence band HAXPES spectra for BaAlSi, SrAlSi, and CaAlSi. The spectra are normalized to the intensity at the binding energy of 10 eV. The inset represents the lattice constants a/b and c for BaAlSi, SrAlSi, and CaAlSi.

in energy. These electrons hybridize with Al $3p_z$ orbitals, leading to bridging the honeycomb layers through a σ-like interaction. Consequently, the anionic electrons are not simply confined in the Ae_3Al_2 cage as discussed in conventional F centers, but give rise to quasi-one-dimensional bonds along the c axis. This anisotropic chemical bond formation results in free-electron-like band dispersion along the Γ-A direction and band flatness along the L-H direction [see Figs. 2(c) and 2(e)]. Indeed, the DFT calculations on the hypothetic $BaAlSiH_{0.5}$ (with plane Al/Si layer) revealed that the k dependence of the interlayer state is highly sensitive to the occupancy of the site X. While the interlayer state contributes to the Fermi level in $BaAlSiH_{0.5}$ as well, the free-electron-like band dispersion along the k_z direction is significantly suppressed (Fig. 7 in Appendix B). We believe that the presence of H impurities destroys the quasi-one-dimensional bond formation between Al $3p_z$ orbitals and site X, fully consistent with the periodic F-center picture in BaAlSi. The emergence of the extra bands with similar k dependence is also seen in both CaAlSi and SrAlSi, implying that this band feature is not unique to BaAlSi but rather is common to this series of the compounds (see Fig. 8).

Support for these theoretical results, including the presence of anionic electrons in the AeAlSi compounds, can be obtained from HAXPES, a spectroscopic technique for probing the bulk electronic structure of materials. In Fig. 3(a), we compare the HAXPES spectrum measured for BaAlSi (on polycrystalline samples in order to collect momentum-independent photoelectrons) with the theoretically calculated total electronic density of states (DOS) distribution. A clear Fermi edge is readily identified in the HAXPES spectrum, pointing to BaAlSi having metallic character. The spectrum shows five clear peaks at 0.44, 1.87, 2.91, 6.59, and 8.45 eV, respectively, in agreement with the calculated DOS in terms of both bandwidths and positions. The peak at 0.44 eV, labeled as X, emerges from the flatness of the anionic electron band along the L-H direction in momentum space, whereas the other four (A, B, C, and D) correspond to the covalent bonding bands derived from the Al/Si 3*s* and 3*p* orbitals. On moving to SrAlSi and CaAlSi [see Figs. 3(b)–3(d)], clear Fermi edges are again seen, and the peak X shifts to a higher binding energy region with reduced relative intensities. It should be noted that the relative intensities of the peaks A and B are also reduced along with X, while the peaks C and D remain essentially unchanged across the AeAlSi series.

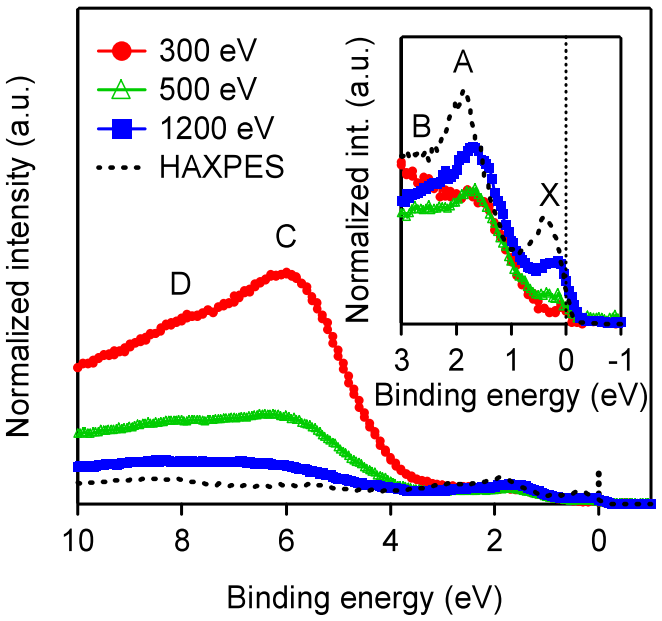

FIG. 4. The valence band SXPES spectra measured using polycrystalline BaAlSi at KEK. The energies of the incident x rays used were $h\nu = 300$, 500, and 1200 eV, respectively. The inset highlights the spectra with binding energy of $-1 < E_B < 3$ eV. Each spectrum was normalized by the Ba core $5p$ peaks located at ~15 eV. The black dashed line represents corresponding HAXPES data measured with $h\nu \sim$ 6000 eV at SPring-8.

These trends can be connected to the structural features of the *Ae*AlSi compounds. Their a and b lattice parameters are tightly tied to the Al-Si bond length, whereas c is a function of the size of the sandwiched metals. Therefore, the lattice parameters a and b are more robust than c against substitution of foreign atoms at the *Ae* site. Such substitution then induces uniaxial chemical pressure along the c axis [see Fig. 3(d) inset]. With increasing uniaxial chemical pressure along the c axis, i.e., from BaAlSi to CaAlSi, the separation between the Al atoms and the interstitial X sites is shortened by ~15%. Consequently, the bandwidth of the bands arising from anionic and Al $3p_z$ electrons are enhanced, with the electronic DOS values then being reduced. This effect accounts for the intensity reduction of both X, A, and B in SrAlSi and CaAlSi. Meanwhile, the Al/Si $3p_{x,y}$ and $3s$ orbitals only contribute to the peaks C and D, both of which undergo negligible intensity change in-line with the inflexibility of the a and b cell parameters.

The orbital character of the interlayer state can be furthermore confirmed by soft x-ray photoemission spectroscopy (SXPES) measurements using different incident photon energies ($h\nu$). In Fig. 4, we compare the SXPES spectra of polycrystalline BaAlSi taken with $h\nu = 300$, 500, 1200, and 6000 eV (HAXPES). Clear Fermi edges as well as characteristic peaks (corresponding to X, A, B, C, and D) were again reproduced for each. It is noteworthy that normalized intensity of the peak X (anionic electrons) enhances with increasing $h\nu$, whereas the peak C (Al/Si $3p_{x,y}$ orbitals) is suppressed. Photoionization cross sections of atomic orbitals, which determine photoelectron intensity, significantly depend on $h\nu$, and their variation is different from each other [33]; i.e., the cross section of s electron relative to p, d electrons increases with the photon energy. These imply that the orbital character of peak X, which shows contrastive intensity modulation to the peak C, is different from Al/Si $3p$ orbitals, excluding the possibility of the π^* scenario discussed previously [14,15], whereas it supports the F-center scenario. Note that the peaks A and B (Al/Si $3p_z$ orbitals) exhibit similar intensity modulation to X, since F-center and Al/Si $3p_z$ electrons exhibit significant orbital hybridization. These data obtained are fully consistent with both HAXPES and DFT studies in which the peaks A and B are suppressed together with X by substituting Ba with Sr and Ca [Fig. 3(d)].

All the measured PES spectra well reproduced theoretical expectations, confirming that anionic electrons play an essential role for realizing the interlayer states in *Ae*AlSi. Such F-center-like electronic states have been discussed before in some ionic solid compounds, including $Cs^+(18C_6)_2(e^-)$ [34], $[Ca_{24}Al_{28}O_{64}]^{4+}(e^-)_4$ [35], and $[Ca_2N]^+(e^-)$ [29], where F-center states emerge between the band gap of the insulating parent phases [36,37] and the anionic electrons are spatially relegated to interstitial spaces with little contribution from the lattice. In contrast, BaAlSiH is a narrow gap semiconductor and the F-center states appear to overlap with the conduction band in energy (Fig. 7). Consequently, anionic electrons contribute to the Fermi surface together with Al $3p_z$ electrons in BaAlSi, and enhance electronic conductance along the interlayer direction. Here, we define the electronic anisotropy ratio as $r_a = m_c^*/m_{ab}^*$, where m_c^* and m_{ab}^* are the effective electron mass along the c and a/b axes estimated from transport data. The r_a values, estimated to be $3 \sim 5$ for *Ae*AlSi [5,38,39], are smaller than those of isostructural, but anionic electron-free, materials, such as MgB_2 ($r_a \sim 25$) [40] and bulk graphite ($r_a \sim 100$) [41]. Given the large interlayer space of BaAlSi, which is greater than 5 Å, it is unlikely that metal-metal bonding along the c axis is responsible for such a reduced electronic anisotropy. Indeed, as is shown in Fig. 5, DFT calculations revealed no obvious signature of orbital overlap between interlayer *Ae* and Si atoms, consistent with earlier theoretical calculations on the hypothetical compound $\square^{2+}$ AlSi ($\square$ = vacant), where interlayer states were found to be present even without *Ae* atoms [42]. Instead, we argue that anionic electrons and Al $3p_z$ orbitals are responsible for the high electronic conductance along the c axis.

The reduced lattice strain after hydrogen incorporation into *Ae*AlSi also supports the presence of anionic electrons. In conventional metals, the formation of hydrides is accompanied by significant unit cell expansion associated with hydrogen insertion into the interstitial site. For instance, in the well-studied hydrogen storage material $LaNi_5$, the unit cell volume is increasingly enlarged by up to a factor of ~1.25 as hydrogen is incorporated [43]. In BaAlSi, on the other hand, the cell volume expansion ratio is one order magnitude smaller than that of $LaNi_5$ [14,43], but very close to those of $[Ca_{24}Al_{28}O_{64}]^{4+}(e^-)_4$ [44] and $[Ca_2N]^+(e^-)$ [45]. It has been proposed that hydrogen atoms may react with anionic electrons involved and can be confined in the vacant site without largely modifying the lattice structure,

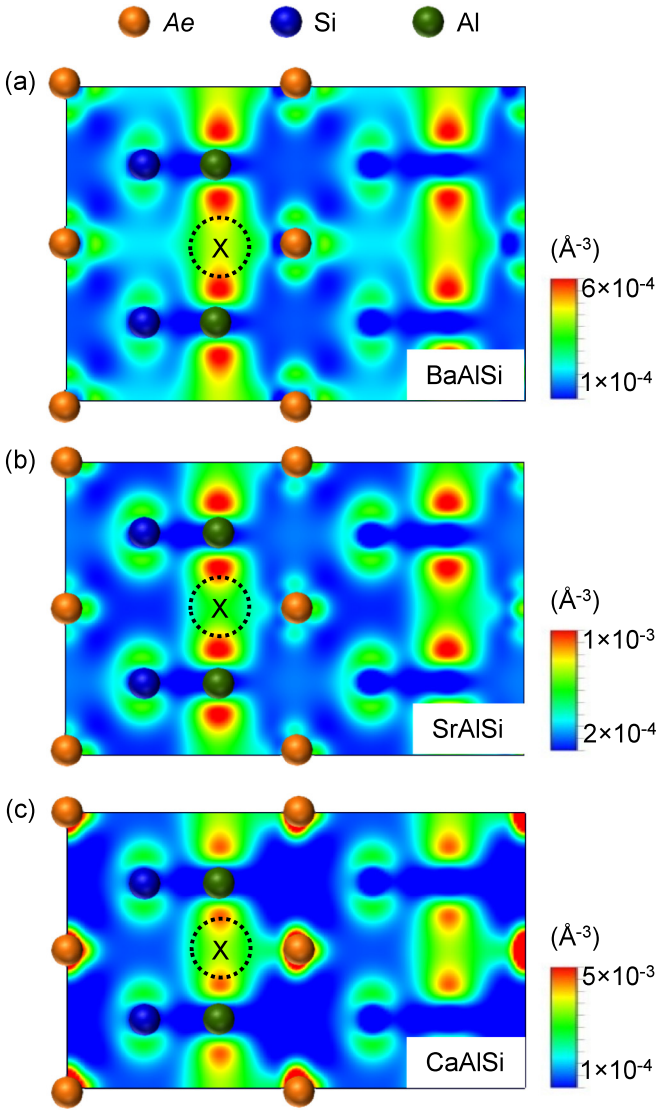

FIG. 5. The electron density map of (a) BaAlSi, (b) SrAlSi, and (c) CaAlSi projected onto the (1 1 0) plane for the states near the Fermi energy. The orange, green, and gray balls represent *Ae*, Al, and Si atoms, respectively. The vacant site X is emphasized using a black dashed circle. The electron density distributions were calculated for states within the energy range of $-0.05 < E - E_F < 0.05$ eV.

reducing the need for cell volume expansion during hydrogen absorption.

Finally, we turn to the possibility of extending the anionic electron picture to the wider range of compounds based on honeycomb layers. We again emphasize that many other compounds in this family, including GICs [11], various metal diborides [11,46,47], and hexagonal BN [48], also host interlayer states with similar k dependence to the extra bands described here. While the interlayer states are located above the Fermi levels in eight valence electron systems, such as MgB_2 [11], hexagonal BN [48], and metal-free graphite (C_2) [9,10], free electrons can be transferred into these interlayer states through electron doping. For instance, the interlayer states clearly cross the Fermi levels in *Ae*AlSi, LiC_2 [11], and YB_2 [46], each of which has nine valence electrons per formula unit. Further increasing the valence electron counts pushes the Fermi level higher up into these interlayer state bands, rather than leading to these states vanishing [47]. These observations imply that the interlayer states are independent of the particular elements involved as long as the crystal structure remains unchanged, fully agreeing with the anionic electron picture in which the periodically distributed cavities themselves serve as extra crystallographic sites.

IV. SUMMARY

The electronic structure of honeycomb lattices is a traditional but still active subject in condensed matter physics. With a combination of DFT calculations and photoemission spectroscopic studies, we have investigated here the interlayer states of the *Ae*AlSi series and interpreted them in terms of anionic electrons. Our work revealed that the *Ae*AlSi compounds host anionic electrons in the Ae_3Al_2 cage that exhibit significant orbital hybridization with Al $3p_z$ orbitals,

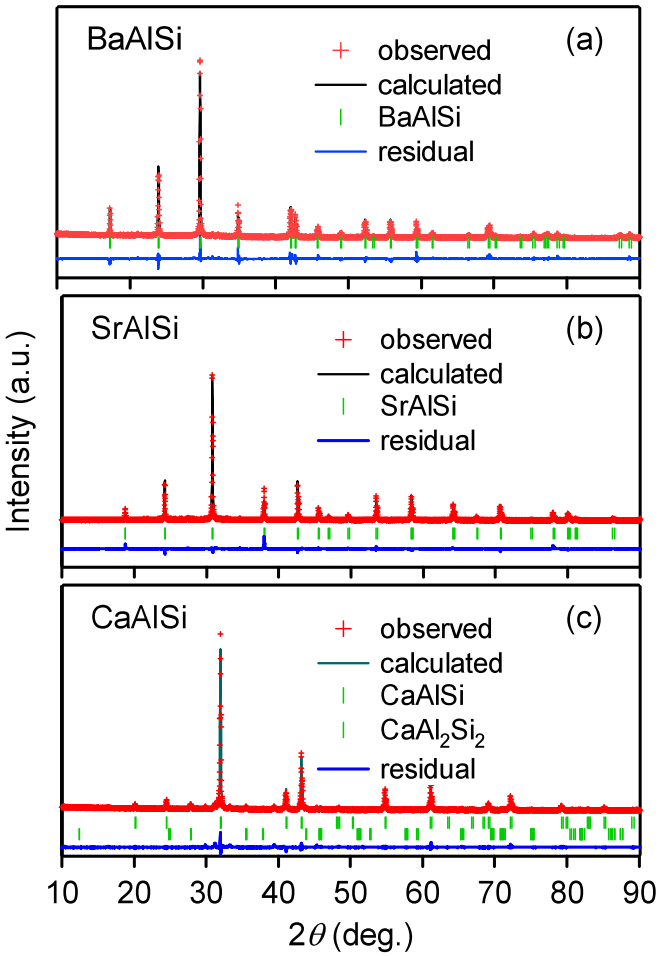

FIG. 6. The powder XRD patterns for (a) BaAlSi, (b) SrAlSi, and (c) CaAlSi taken at room temperature. The red crosses, black solid line, green bars, and blue solid line represent the experimental data, calculated pattern, Bragg positions, and the residual of Rietveld refinement, respectively. The reliability parameters are $R_{wp} = 11.770\%, R_e = 5.965\%$ for BaAlSi, $R_{wp} = 8.600\%, R_e = 3.952\%$ for SrAlSi, and $R_{wp} = 12.005\%, R_e = 5.880\%$ for CaAlSi.

giving rise to additional bands with free-electron-like dispersion along the k_z direction. These findings cannot be interpreted within any of the previously established models for the interlayer states of these compounds, and therefore deliver a new picture that applies the anionic electron concept to the electronic structures of a range of honeycomb lattice compounds.

ACKNOWLEDGMENTS

The authors are grateful to Prof. T. Inoshita and Prof. D. C. Fredrickson for useful discussions and their critical reading of the manuscript. The project was supported by Ministry of Education, Culture, Sports, Science and Technology (MEXT) Element Strategy Initiative and ACCEL of JST in Japan. The HAXPES measurements were performed with the approval of NIMS Synchrotron X-ray Station (Proposals No. 2015A4703 and No. 2015B4703). S.U. is grateful to HiSOR (Hiroshima University) and JAEA/SPring-8 for the development of HAXPES at BL15XU of SPring-8. The work at KEK-PF was performed under the approval of the Program Advisory Committee (Proposals No. 2013S2-002 and No. 2015S2-005) at the Institute of Materials Structure Science, KEK.

Y.F.L. and T.T. contributed equally to this paper.

APPENDIX A: SAMPLE CHARACTERIZATIONS

In order to evaluate the sample quality of polycrystalline *Ae*AlSi, we conducted powder XRD and Rietveld analysis. In Fig. 6, we shows the powder XRD patterns of each *Ae*AlSi. The obtained spectra were well refined using the SrPtSb-type (P-6m2, No. 187) structure. The refined lattice parameters were $a = b = 4.185(3)$ Å and $c = 4.394(0)$ Å for CaAlSi, $a = b = 4.245(9)$ Å and $c = 4.743(7)$ Å for SrAlSi, and $a = b = 4.295(7)$ Å and $c = 5.144(9)$ Å for BaAlSi. While single phases of BaAlSi and SrAlSi were obtained, ∼3 wt.% of $CaAl_2Si_2$ can be identified as an impurity phase in CaAlSi. The refined lattice parameters agree well with the computationally optimized values and the previous reported data [14], and these parameters are summarized in Table I.

TABLE I. The experimentally refined and computationally optimized lattice parameters.

	Rietveld		DFT	
	a, b (Å)	c (Å)	a, b (Å)	c (Å)
BaAlSiH	4.3186(4)[a]	5.2080(9)[a]	4.33697	5.24243
BaAlSi	4.295(7)	5.144(9)	4.32746	5.17163
SrAlSi	4.245(9)	4.743(7)	4.26990	4.74988
CaAlSi	4.185(3)	4.394(0)	4.21110	4.38890

[a]Reference [14].

APPENDIX B: ELECTRONIC STRUCTURE CALCULATIONS

In Fig. 7, we show the calculated band structures of BaAlSiH, $BaAlSiH_{0.5}$, and BaAlSi with plane Al/Si layers for comparison. The Al/Si $3p_{x,y}$, Al/Si $3p_z$, and vacant electrons are depicted using red, blue, and green dots, respectively. The calculated band structures of each *Ae*AlSi and the contributions of particular orbitals are summarized in Fig. 8. All of the *Ae*AlSi compounds host interlayer states that originate from the vacant site X.

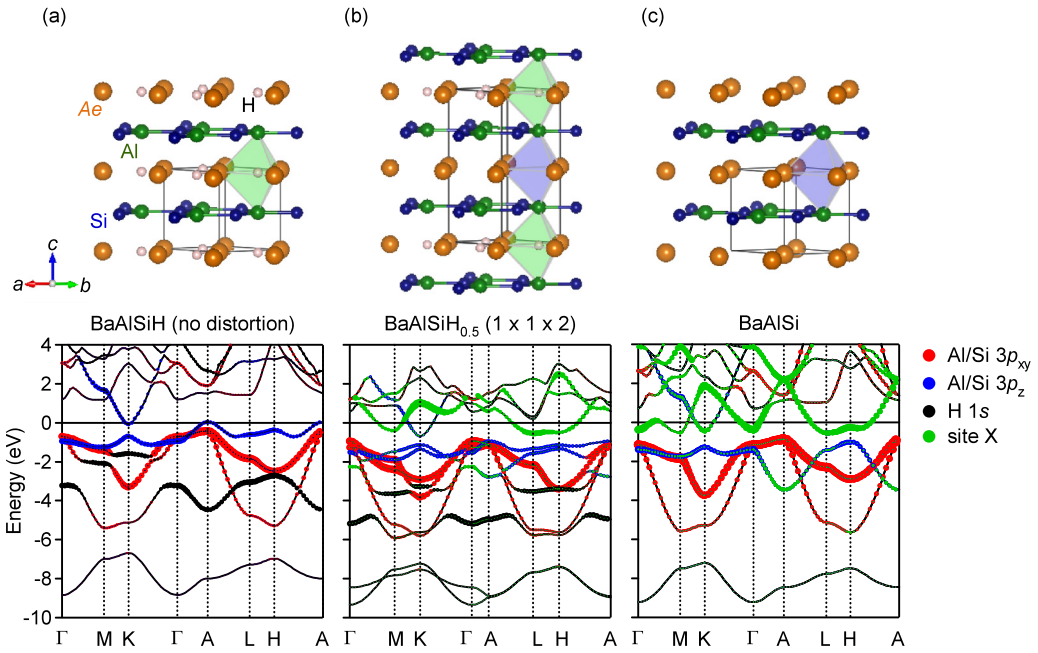

FIG. 7. The crystal structures and calculated band structures of hypothetic (a) BaAlSiH, (b) $BaAlSiH_{0.5}$, and (c) real BaAlSi. The contributions of Al/Si $3p_{xy}$, Al/Si $3p_z$, H 1s orbitals and vacant site X are represented using, red, blue, black, and green dots, respectively. The crystal structures of both BaAlSiH and $BaAlSiH_{0.5}$ used in the calculations are based on BaAlSi with plane Al/Si layers. The green and blue polyhedra indicate Ba_3Al_2H and Ba_3Al_2X cages, respectively.

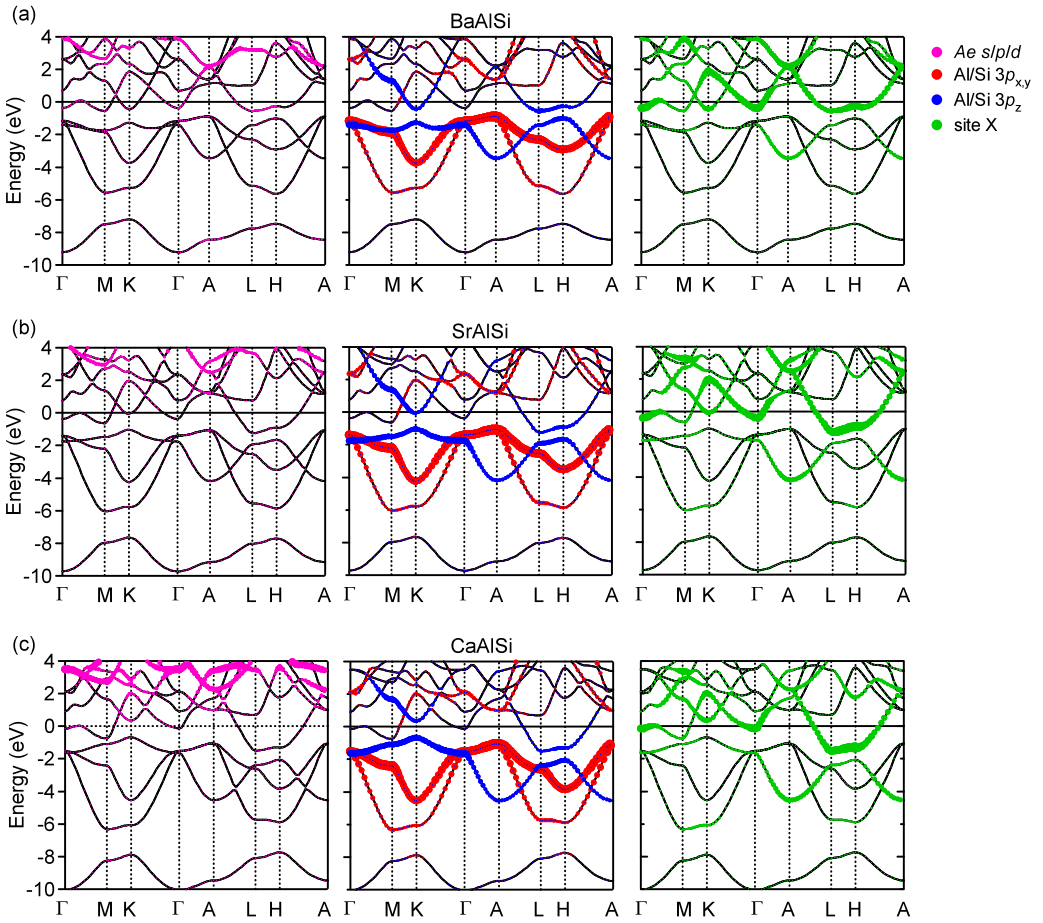

FIG. 8. Calculated band structures of (a) BaAlSi, (b) SrAlSi, and (c) CaAlSi. The contributions of Ae, Al/Si $3p_{xy}$, Al/Si $3p_z$ orbitals and vacant site X are represented using purple, red, blue, and green dots.

[1] K. S. Novoselov, A. K. Geim, S. V. Morozov, D. Jiang, M. I. Katsnelson, I. V. Grigorieva, S. V. Dubonos, and A. A. Firsov, Nature (London) **438**, 197 (2005).

[2] Y. Zhang, Y. W. Tan, H. L. Stormer, and P. Kim, Nature (London) **438**, 201 (2005).

[3] J. Nagamatsu, N. Nakagawa, T. Muranaka, Y. Zenitani, and J. Akimitsu, Nature (London) **410**, 63 (2001).

[4] B. Lorenz, J. Cmaidalka, R. L. Meng, and C. W. Chu, Phys. Rev. B **68**, 014512 (2003).

[5] S. Kuroiwa, T. Kakiuchi, H. Sagayama, H. Sawa, and J. Akimitsu, Physica C **460-462**, 154 (2007).

[6] T. E. Weller, M. Ellerby, S. S. Saxena, R. P. Smith, and N. T. Skipper, Nat. Phys. **1**, 39 (2005).

[7] S. Heguri, N. Kawade, T. Fujisawa, A. Yamaguchi, A. Sumiyama, K. Tanigaki, and M. Kobayashi, Phys. Rev. Lett. **114**, 247201 (2015).

[8] J. S. Kim, L. Boeri, J. R. O'Brien, F. S. Razavi, and R. K. Kremer, Phys. Rev. Lett. **99**, 027001 (2007).

[9] M. Posternak, A. Baldereschi, A. J. Freeman, E. Wimmer, and M. Weinert, Phys. Rev. Lett. **50**, 761 (1983).

[10] Th. Fauster, F. J. Himpsel, J. E. Fischer, and E. W. Plummer, Phys. Rev. Lett. **51**, 430 (1983).

[11] G. Csányi, P. B. Littlewood, A. H. Nevidomskyy, C. J. Pickard, and B. D. Simons, Nat. Phys. **1**, 42 (2005).

[12] K. Kanetani, K. Sugawara, T. Sato, R. Shimizu, K. Iwaya, T. Hitosugi, and T. Takahashi, Proc. Natl. Acad. Sci. USA **109**, 19610 (2012).

[13] I. I. Mazin and D. A. Papaconstantopoulos, Phys. Rev. B **69**, 180512(R) (2004).

[14] M. H. Lee, T. Björling, B. C. Hauback, T. Utsumi, D. Moser, D. Bull, D. Noréus, O. F. Sankey, and U. Häussermann, Phys. Rev. B **78**, 195209 (2008).

[15] I. R. Shein, V. V. Ivanovskaya, N. I. Medvedeva, and A. L. Ivanovskii, JETP Lett. **76**, 189 (2002).

[16] T. Sato, Y. X. Xiao, S. Souma, K. Nakayama, K. Sugawara, S. Kuroiwa, J. Akimitsu, and T. Takahashi, Phys. Rev. B **91**, 195114 (2015).

[17] S. L. Yang, J. A. Sobota, C. A. Howard, C. J. Pickard, M. Hashimoto, D. H. Lu, S. K. Mo, P. S. Kirchmann, and Z. X. Shen, Nat. Commun. **5**, 3493 (2014).

[18] M. Calandra and F. Mauri, Phys. Rev. Lett. **95**, 237002 (2005).

[19] S. Kuroiwa, A. Q. R. Baron, T. Muranaka, R. Heid, K. P. Bohnen, and J. Akimitsu, Phys. Rev. B **77**, 140503(R) (2008).

[20] S. Deng, A. Simon, and J. Köhler, Angew. Chem. Int. Ed. **47**, 6703 (2008).

[21] H. Okazaki, R. Yoshida, K. Iwai, K. Noami, T. Muro, T. Nakamura, T. Wakita, Y. Muraoka, M. Hirai, F. Tomioka,

Y. Takano, A. Takenaka, M. Toyoda, T. Oguchi, and T. Yokoya, Phys. Rev. B **80**, 035420 (2009).
[22] S. L. Molodtsov, C. Laubschat, M. Richter, Th. Gantz, and A. M. Shikin, Phys. Rev. B **53**, 16621 (1996).
[23] F. Karsai, P. Tiwald, R. Laskowski, F. Tran, D. Koller, S. Gräfe, J. Burgdörfer, L. Wirtz, and P. Blaha, Phys. Rev. B **89**, 125429 (2014).
[24] D. L. Dexter, Phys. Rev. **83**, 435 (1951).
[25] F. Izumi and K. Momma, Solid State Phenom. **130**, 15 (2007).
[26] K. Momma and F. Izumi, J. Appl. Crystallogr. **44**, 1272 (2011).
[27] J. P. Perdew, K. Burke, and M. Ernzerhof, Phys. Rev. Lett. **77**, 3865 (1996).
[28] G. Kresse and J. Furthmüller, Phys. Rev. B **54**, 11169 (1996).
[29] K. Lee, S. W. Kim, Y. Toda, S. Matsuishi, and H. Hosono, Nature (London) **494**, 336 (2013).
[30] S. Ueda, Y. Katsuya, M. Tanaka, H. Yoshikawa, Y. Yamashita, S. Ishimaru. Y. Matsushita, and K. Kobayashi, AIP Conf. Proc. **1234**, 403 (2010).
[31] S. Ueda, J. Electron Spectrosc. Relat. Phenom. **190**, 235 (2013).
[32] E. A. Stern, Phys. Rev. **157**, 544 (1967).
[33] J. J. Yeh and I. Lindau, At. Data Nucl. Data Tables **32**, 1 (1985).
[34] A. Ellaboudy, J. L. Dye, and P. B. Smith, J. Am. Chem. Soc. **105**, 6490 (1983).
[35] S. Matsuishi, Y. Toda, M. Miyakawa, K. Hayashi, T. Kamiya, M. Hirano, I. Tanaka, and H. Hosono, Science **301**, 626 (2003).
[36] P. V. Sushko, A. L. Shluger, K. Hayashi, M. Hirano, and H. Hosono, Phys. Rev. Lett. **91**, 126401 (2003).
[37] S. G. Dale, A. Otero-de-la-Rozaa, and E. R. Johnsona, Phys. Chem. Chem. Phys. **16**, 14584 (2013).
[38] M. Imai, E. S. Sadki, H. Abe, K. Nishida, T. Kimura, T. Sato, K. Hirata, and H. Kitazawa, Phys. Rev. B **68**, 064512 (2003).
[39] T. Nakagawa, M. Tokunaga, and T. Tamegai, Sci. Technol. Adv. Mater. **7**, S108 (2006).
[40] L. Lyard, P. Samuely, P. Szabo, T. Klein, C. Marcenat, L. Paulius, K. H. P. Kim, C. U. Jung, H.-S. Lee, B. Kang, S. Choi, S. I. Lee, J. Marcus, S. Blanchard, A. G. M. Jansen, U. Welp, G. Karapetrov, and W. K. Kwok, Phys. Rev. B **66**, 180502(R) (2002).
[41] P. R. Wallace, Phys. Rev. **71**, 622 (1947).
[42] M. Giantomassi, L. Boeri, and G. B. Bachelet, Phys. Rev. B **72**, 224512 (2005).
[43] T. Sakai, K. Oguro, H. Miyamura, N. Kuriyama, A. Kato, H. Ishikawa, and C. Iwakura, J. Less Common Metals **161**, 193 (1990).
[44] K. Hayashi, P. V. Sushko, Y. Hashimoto, A. L. Shluger, and H. Hosono, Nat. Commun. **5**, 3515 (2014).
[45] O. Reckeweg and F. J. DiSalvo, Solid State Sciences **4**, 575 (2002).
[46] N. I. Medvedeva, A. L. Ivanovskii, J. E. Medvedeva, and A. J. Freeman, Phys. Rev. B **64**, 020502(R) (2001).
[47] I. R. Shein and A. L. Ivanovskii, Phys. Solid State **44**, 1833 (2002).
[48] A. Catellani, M. Posternak, A. Baldereschi, H. J. F. Jansen, and A. J. Freeman, Phys. Rev. B **32**, 6997(R) (1985).